Chinese Chemical Letters 37 (2026) 111414

Contents lists available at ScienceDirect

Chinese Chemical Letters

journal homepage: www.elsevier.com/locate/cclet

Redox and conductive covalent-organic binding agent boosts sulfur conversion kinetics in Li-S batteries

Taoping Huang[a,1], Xiaoman Yao[a,1], Xuanxu Chen[a], Minqiao Liang[a], Mingjin Shi[a], Yiwen Yang[a], Fei Yu[b], Fengxue Duan[a,*], Yifa Chen[a,*], Ya-Qian Lan[a]

[a] Guangdong Provincial Key Laboratory of Carbon Dioxide Resource Utilization, School of Chemistry, South China Normal University, Guangzhou 510006, China
[b] School of Chemistry and Materials Science, Nanjing Normal University, Nanjing 210023, China

ARTICLE INFO

Article history:
Received 22 March 2025
Revised 29 May 2025
Accepted 6 June 2025
Available online 6 June 2025

Keywords:
Tetrathiafulvalene
Binder
Redox ability
Conductivity
Li-S battery

ABSTRACT

Integration of redox ability and conductivity in binder is highly desirable to maximize their functions for high-performance battery requirements. Here, a novel redox covalent organic polymer binder (TTF-COP) has been developed by *in-situ* polymerizing redox/conductive tetrathiafulvalene unit and adhesive thiourea unit. TTF-COP can achieve one-pot cathode fabrication and simultaneously provide strong interactions with cathodic materials, showing significantly enhanced mechanical strength of the electrode, accelerated capture/conversion of lithium polysulfides (LiPSs), about 10,000 times higher viscosity (at shear rates of 0.1–1 s^{-1}), and about 200 times enhanced electrical conductivity than that of PVDF. TTF-COP based cells exhibit high initial capacity (1126 mAh/g at 0.5 C, 928 mAh/g at 1 C, 611 mAh/g at 5 C, respectively) and excellent cycling stability over 800 cycles at 5 C (0.089 % decay per cycle). Moreover, the cell shows an excellent specific capacity of 5.1 mAh/cm^2 under a high sulfur loading of 7.1 mg/cm^2 and low E/S ratio of 10.7 μL/mg. This work provides a new reference for designing multifunctional binders, hoping to enrich the binding chemistry for sustainable battery targets.

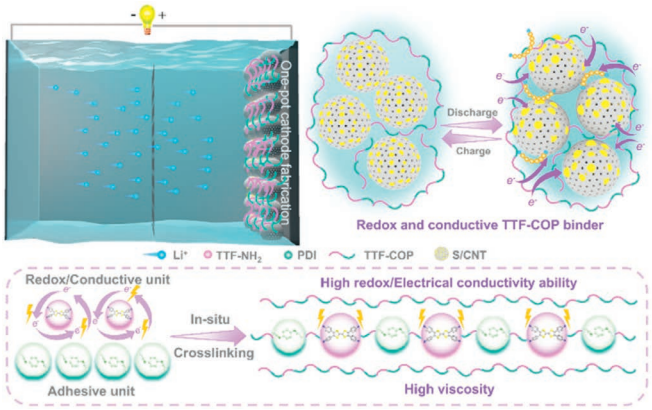
© 2026 Published by Elsevier B.V. on behalf of Chinese Chemical Society and Institute of Materia Medica, Chinese Academy of Medical Sciences.

Lithium-sulfur batteries (LSBs) have been considered as the next generation rechargeable batteries used in practical applications owing to its large theoretical specific energy (2567 Wh/kg) and capacity (1675 mAh/g) [1,2]. In addition, the low cost (<$200 ton^{-1}), the abundant source and the friendly environmental impact of sulfur endow LSBs with more commercial competitiveness [3–5]. However, LSBs still face several challenges, such as the shedding of active material during cycling, the shuttle effect of lithium polysulfides (LiPSs), and the slow deposition and dissolution of Li_2S, which result in unmet performances for potential commercialization [6,7]. To address these critical issues, many works focused on the optimizing key components of LSBs like host materials, electrolytes, separators and binders [8–11]. The binder, although accounting for <10 wt% in LSBs, has garnered significant attention over the past few decades [12,13]. It not only provides the essential function of adhesion but also plays a crucial role in various aspects, such as maintaining the integrity of electrode structure, adsorbing and catalyzing LiPSs, and facilitating Li^+ hoping and transfer [14–16]. In general, poly(vinylidene fluoride) PVDF is considered as the most mature and commercialized binder due to its affordability, moderate mechanical stability and electrochemical stability, while it still exhibits poor electric conductivity, as well as inadequate viscosity and mechanical strength for high performance batteries due to its semicrystalline polymeric nature [17–19]. To date, some advanced functions have been introduced into polymer binders, including mechanical property (*e.g.*, FBCP binder and PLG binder) [20,21], conductivity (*e.g.*, LVCA binder and FNA binder) [22,23] and LiPSs regulation ability (*e.g.*, ZIP binder and iPANI binder) [24,25]. However, there are still some challenges for the reported binders, such as: (1) Sluggish kinetics in redox process; (2) lacked in physical space confinement and chemical adsorption for suppressing LiPSs migration and (3) the balance between electric conductivity and mechanical properties. Therefore, it would be much desired to design novel binders with advanced functions to meet the sustainable battery requirements.

In view of these challenges, tetrathiafulvalene (TTF), a sulfur-rich conjugated organic molecule with 14 π electrons that has stimulated intensive interest owing to its excellent redox properties, comes to our mind as an alternative construction unit for binder design [26–29]. In this context, we have considered the de-

* Corresponding authors.
E-mail addresses: dfx0118@163.com (F. Duan), chyf927821@163.com (Y. Chen).
[1] These authors contributed equally to this work.

https://doi.org/10.1016/j.cclet.2025.111414
1001-8417/© 2026 Published by Elsevier B.V. on behalf of Chinese Chemical Society and Institute of Materia Medica, Chinese Academy of Medical Sciences.



Scheme 1. The schematic illustration of advantages of TTF-COP as binder in Li-S battery.

sign of functional binder based on the combination of TTF and thiourea units based on the following considerations: (1) As an important redox radical molecule with 14 π electrons, TTF unit can serve as a π-electron donor unit in catalyzing and adsorbing LiPSs to address the slow reaction kinetics of LiPSs [30–32]; (2) as a conjugated organic molecule, TTF unit demonstrates good electrochemical stability and high electrical conductivity [27,33] and (3) thiourea unit has been proven to be ideal adhesive unit in enhancing the binding ability of binders [11,34]. Thus, the combination of TTF unit with thiourea unit might result in binder with high viscosity, robust mechanical strength, strong LiPSs adsorptive/catalytic capabilities, and high electrical conductivity, while it is still rare in designing such interesting binders as far as we knew.

Herein, we report a novel redox covalent organic polymer binder (tetrathiafulvalene covalent organic polymer, TTF-COP) by *in-situ* polymerizing redox/conductive tetrathiafulvalene unit and adhesive thiourea unit (Scheme 1). TTF-COP can achieve one-pot cathode fabrication and simultaneously provide strong interactions with cathodic materials, showing significantly enhanced mechanical strength of the electrode, accelerated capture/conversion of LiPSs, $\sim 10^4$ times higher viscosity (at shear rates of 0.1–1 s^{-1}) and $\sim$200 times enhanced electrical conductivity than that of PVDF [35–38]. The TTF-COP based battery delivers initial specific capacities of 1126, 928, 611 mAh/g at 0.5, 1 and 5 C, respectively, and excellent cycling stability over 800 cycles at 5 C (0.089 % decay per cycle and the Coulombic efficiency is nearly 100 %). Specifically, it also delivers outstanding cycling performance (5.1 mAh/cm^2 at 0.1 C) under high sulfur-loading (7.1 mg/cm^2) and a low E/S ratio (10.2 μL/mg). Validated by the theoretical calculation, the vital roles of TTF and thiourea units in facilitating the capture/conversion of LiPSs have been intensively studied by the density functional theory (DFT) calculation and sufficient characterizations.

TTF-COP was prepared by a facile thermal polymerization reaction through the assembly of tetrathiafulvalene tetraphenylamine ($TTF\text{-}NH_2$) and 1,4-diisocyanate (PDI) (Fig. 1a, details see Supporting information). Interestingly, the obtained TTF-COP can be processed in the forms of gel, powder and film (Fig. 1b and Fig. S1 in Supporting information). As illustrated in Fig. 1b, the image of TTF-COP film reveals a self-supporting and homogeneous morphology over a large surface area. The powder X-ray diffraction (PXRD) pattern of TTF-COP exhibits amorphous characteristic without any detectable crystalline phase, validating its amorphous polymeric nature (Fig. 1c). In addition, Fourier transform infrared (FTIR) spectroscopy confirms the formation of thiourea bond in TTF-COP ($\nu_{thiourea}$ at 1500 cm^{-1}) and disappearance of isothiocyanate in PDI ($\nu_{isothiocyanate}$ at 2000–2200 cm^{-1}) and N–H in $TTF\text{-}NH_2$ (3350 cm^{-1}), indicating the combination of two components (Fig. 1d) [11,39]. Furthermore, the solid-state ^{13}C NMR spectrum of TTF-COP is assigned to the relative carbon atoms in TTF unit (**a**, **b**, **c**, **d** and **e**), thiourea unit (**f**) and PDI unit (**g**) (Fig. 1e). It displays a characteristic peak (175 ppm) of C=S for thiourea unit, which also proves the covalent bonding between $TTF\text{-}NH_2$ and PDI, consistent with above FTIR results [28,40,41]. In addition, X-ray photoelectron spectroscopy (XPS) was applied to investigate the elemental valence states and chemical composition of TTF-COP. Three major peaks of 284.6, 400.0 and 162.8 eV are assigned to C 1s, N 1s, and S 2p, respectively (Figs. S2 and S3 in Supporting information) [42]. The C 1s signals (*i.e.*, C=C, C–N, and C=S peaks at 284.8, 285.9 and 287.7 eV, respectively) of PDI and $TTF\text{-}NH_2$ monomers are observed in TTF-COP, which further reveal the presence of two monomers [11,40]. In addition, the elemental mapping images of TTF-COP demonstrate evenly distribution of C, S and N elements (Fig. S4 in Supporting information). To highlight the redox/conductive properties of TTF units in covalent organic polymer binders, TPA-COP (phenyltetraphenylamine covalent organic polymer) was synthesized by replacing the TTF units with TPA units and characterized (Figs. S5-S9 in Supporting information).

Mechanical strength is an important parameter for evaluating the adhesive ability to suppress the volume change of electrode

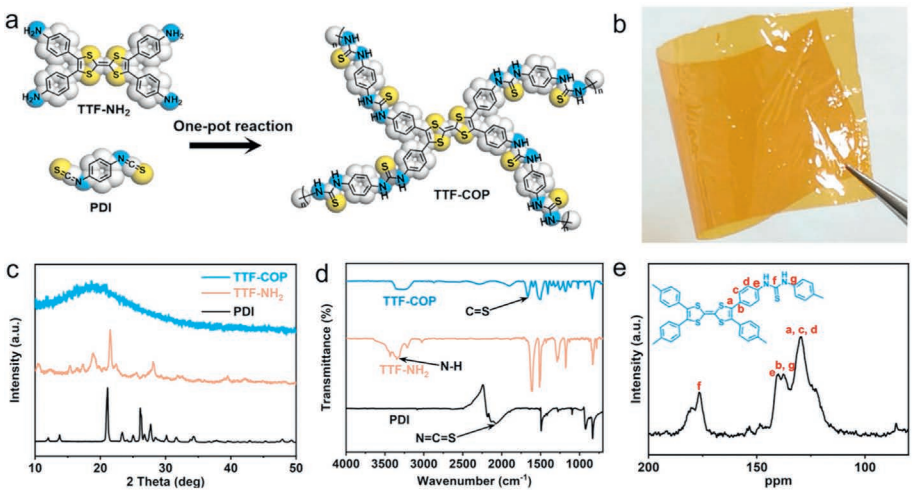


Fig. 1. Structure and characterization of TTF-COP. (a) The synthesis process of TTF-COP. (b) The photograph of TTF-COP film. (c) The PXRD patterns of TTF-COP, PDI and $TTF\text{-}NH_2$. (d) The FTIR spectra of TTF-COP, $TTF\text{-}NH_2$ and PDI. (e) Solid-state ^{13}C CP/MAS NMR spectrum of TTF-COP.

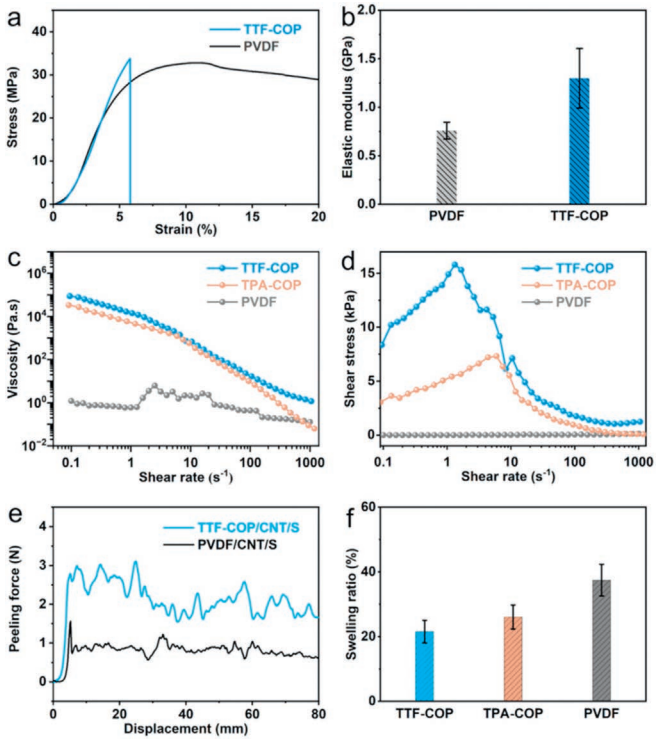


Fig. 2. Mechanical strength characterizations of different binders. (a) Stress-strain curves of TTF-COP and PVDF. (b) Elastic modulus of TTF-COP and PVDF. (c) Viscosity as a function of shear rate for TTF-COP and PVDF. (d) Shearing adhesion strength of TTF-COP and PVDF. (e) Peel-off strength profiles of TTF-COP/CNT/S and PVDF/CNT/S electrodes. (f) Swelling ratios of TTF-COP/CNT/S, TPA-COP/CNT/S and PVDF/CNT/S electrodes.

during cycling. The stress-strain results reveal the maximum tensile stress of TTF-COP is 33.81 MPa (strain = 5.8 %), which is slightly higher than that of PVDF (stress, 32.97 MPa; strain, 10.7 %) (Fig. 2a). Although the elongation at break (5.8 %) of TTF-COP is inferior to that of PVDF, the elastic modulus of TTF-COP (1.30 GPa) is nearly twice higher than that of PVDF (0.76 GPa) (Fig. 2b), indicating the notable comprehensive mechanical capacity of TTF-COP [43,44]. Moreover, the dynamic shear rheological characteristic of binder plays a crucial role in resisting the volumetric deformation of cathode and maintaining structural stability in LSBs. The results show that TTF-COP has noticeably superior viscosity of 10^4 Pa s at shear rates of 0.1–1 s^{-1}, which is approximately 10^4 times higher than that of PVDF (Fig. 2c). Among the same shear rate range, its shear strength is about 10^4 Pa, approximately 10^4 times higher than that of PVDF (Fig. 2d) [45,46]. Furthermore, TPA-COP also exhibits superior mechanical strength compared to PVDF (Figs. S10 and S11 in Supporting information). Besides, the folding tests demonstrate the macroscopic adhesion of TTF-COP, during which no material detached from the electrode and no visible creases are observed, validating better adhesiveness and dynamic stable characteristics compared to PVDF (Figs. S12 and S13 in Supporting information). Moreover, other properties of TTF-COP, as a novel binder of LSBs, are further explored. The adhesiveness of TTF-COP has been assessed, using 180° peeling tests at a stretching velocity of 0.17 mm/s, with PVDF as a contrast (Fig. 2e) [47,48]. It is found that, for a given same displacement, the TTF-COP/CNT/S electrode requires a greater force. The strong adhesion of TTF-COP can effectively prevent the peeling and falling of the electrode materials. The stability of the binder after immersion in the electrolyte is also a key factor for long-term cycling. During this process, moderate electrode swelling would prevent excessive electrolyte absorption and simultaneously maintain the good wettability of the electrolyte [13]. The electrodes, assembled with TTF-COP and PVDF, were soaked in the electrolyte for 24 h to test their swelling resistance. The results reveal that the electrode with PVDF (37.5 %) was prone to swelling compared to others (TTF-COP, 23.5 % and TPA-COP, 26.1 %) (Fig. 2f). To further determine their mechanical strength and adhesion properties, nano-indentation tests of TTF-COP/CNT/S and PVDF/CNT/S electrodes were then studied. When the indentation depth is 2000 nm, the TTF-COP/CNT/S electrode requires a higher applied force, indicating the increased hardness, which allows it to withstand greater external pressure without deformation. Additionally, the TTF-COP/CNT/S electrode (0.49 GPa) exhibits higher elastic modulus than that of PVDF/CNT/S (0.36 GPa) (Fig. S14 in Supporting information) [49].

Based on the above-mentioned results, TTF-COP can serve as both a binding agent for cathode and redox-active agent for the adsorption/conversion of LiPSs. To prove it, the adsorption tests were conducted by adding the same amount of TTF-COP and PVDF into Li_2S_6 solution. After 24 h, the transparent solution was observed by TTF-COP, signifying the adsorption capacity of TTF-COP for LiPSs (Fig. 3a) [50,51]. The intensity of UV–vis absorption spectrum in the range of 250–300 nm witnesses extreme decline for the Li_2S_6 solution, further confirming above results (Fig. 3a). Furthermore, the XPS test was conducted to confirm the chemical interaction between TTF-COP and LiPSs during the adsorption tests. Fig. 3b shows the S 2p XPS results of TTF-COP before and after Li_2S_6 adsorption. The S 2p XPS of TTF-COP before Li_2S_6 adsorption at 161.9 eV is attributed to the thiourea group [11,52]. In contrast, After adsorption, terminal sulfur (S_T^{-1}) and bridging sulfur (S_B^0) of LiPSs also appear at 161.9 and 163.1 eV, overlapping with the original peaks [53,54]. And the appearance of Li 1s XPS in TTF-COP/Li_2S_6 composites was also detected, ascribed to the strong adsorption between TTF-COP and LiPSs (Figs. S15 and S16 in Supporting information). To investigate the interfacial charge transfer kinetics, the electrochemical impedance spectroscopy (EIS) was studied. The TTF-COP/CNT/S electrode presents the smallest charge transfer resistance (R_{ct}) before cycling, indicating better ion conductivity and faster electrochemical reactions within the battery, thereby enhancing the overall performance (Figs. S17 and S18 in Supporting information).

With the above considerations, DFT calculation has been performed to understand the crucial role of TTF-COP during the battery performance (Figs. S19-S22 in Supporting information). The Li atoms in Li_2S are in close proximity to the sulfur atoms in TTF, which significantly activates the Li-S bonds to promote the adsorption and conversion of Li_2S (Fig. 3c). The higher binding energy of LiPSs on TTF-COP compared to TPA-COP and PVDF, demonstrating a stronger affinity of LiPSs towards TTF-COP (Fig. 3f). In the reversible conversion between S_8 and Li_2S, a more negative Gibbs free energy is a higher likelihood of spontaneous reaction proceeding [16]. By comparison, the $Li_2S_2 \rightarrow Li_2S$ reaction has the highest positive Gibbs free energy, indicating that this is the rate determining step (Fig. 3e). Therefore, Fig. 3d calculates the more negative ΔG_{max} value for TTF-COP in the key reaction ($Li_2S_2 \rightarrow Li_2S$), indicating that TTF-COP significantly promotes the catalytic conversion of LiPSs than PVDF in the reaction process. Furthermore, the sulfur conversion process during the discharge of Li-S batteries is divided into five stages, the more negative reaction energy value indicates the easier chemical reaction. It proves that the introduction of TTF-COP is able to lower the energies required for various sulfur conversion reactions and especially promote the rate-limiting liquid–solid conversion reactions (entries R4 and R5, Fig. S23 and Table S1 in Supporting information) [55,56]. Above all, TTF-COP not only enhances the adsorption of Li_2S but also promotes the rapid catalytic conversion of LiPSs in the DFT calculation, which is consistent with the previously mentioned experimental results [26,29–32]. Furthermore, the redox kinetics of LiPSs plays a sig-

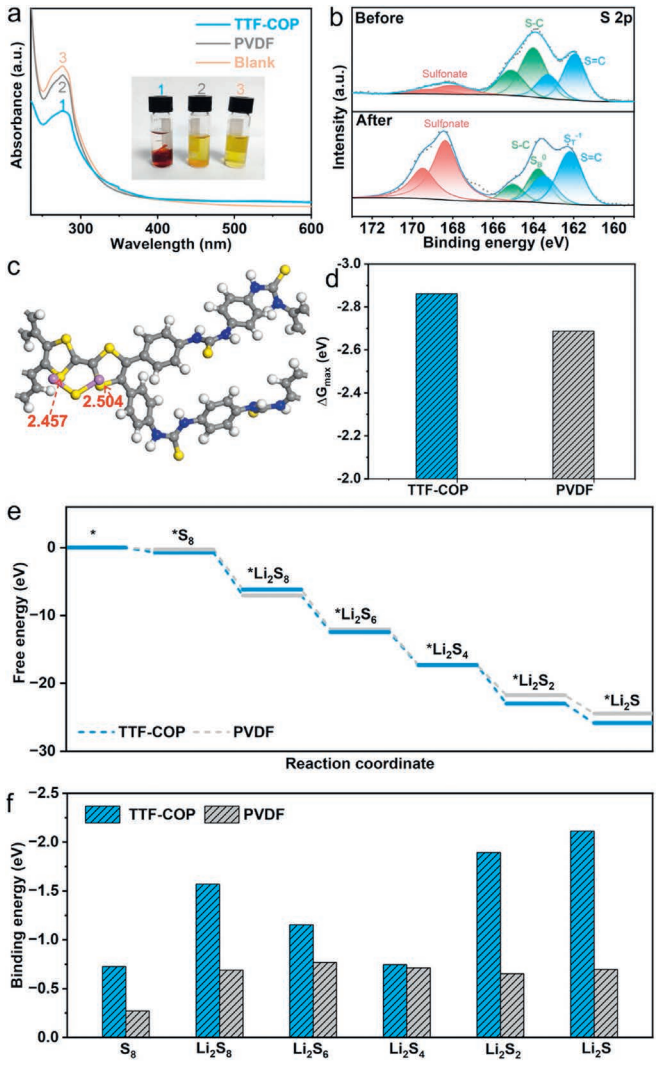


Fig. 3. Adsorption and conversion reactions of LiPSs and DFT calculation of different binders. (a) Images and UV–vis spectra of Li_2S_6 adsorption on PVDF and TTF-COP in DOL/DME solution. (b) S 2p XPS spectra of TTF-COP before and after Li_2S_6 adsorption. (c) The collective results of bond length of S-Li between the adsorbed Li_2S and TTF-COP. (d) The ΔG_{max} values for the highest positive Gibbs free energy ($Li_2S_2 \rightarrow Li_2S$) on TTF-COP and PVDF. (e) The reaction free energy diagrams. (f) The binding energy of S_8 and Li_2S_x ($1 \leq x \leq 8$) on TTF-COP and PVDF.

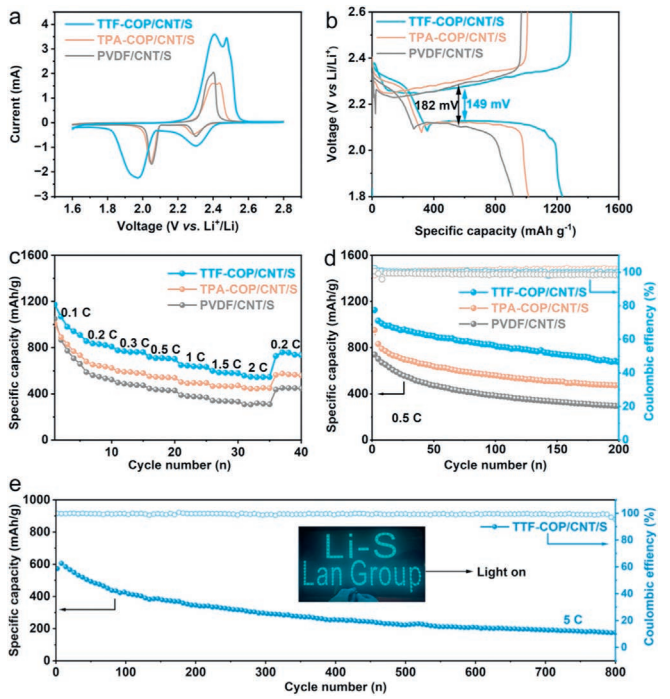


Fig. 4. Electrochemical performances of LSBs with different binders. (a) CV curves of TTF-COP/CNT/S, TPA-COP/CNT/S and PVDF/CNT/S at a scanning rate of 0.1 mV/s in the voltage range of 1.6–2.8 V. (b) Charge–discharge curves of TTF-COP/CNT/S, TPA-COP/CNT/S and PVDF/CNT/S at 0.5 C. (c) Rate performances of LSBs with TTF-COP/CNT/S, TPA-COP/CNT/S and PVDF/CNT/S. (d) Cycling performances of TTF-COP/CNT/S, TPA-COP/CNT/S and PVDF/CNT/S at 0.5 C. (e) Cycling performance of TTF-COP/CNT/S at 5 C.

nificant role in high performance LSBs. Thus, the redox kinetics of LiPSs were studied by Li_2S nucleation tests. The calculated capacities of Li_2S with the TTF-COP, and PVDF are 253.4 and 116.0 mAh/g, respectively, verifying that the TTF-COP binder facilitates the fast Li_2S nucleation and deposition. In addition, the TTF-COP binder exhibits higher current intensity and earlier time of Li_2S nucleation than PVDF binder, indicating its faster conversion redox kinetics (Fig. S24 in Supporting information) [57–61]. Interestingly, the electrical conductivity of TTF-COP and PVDF in the form of film was also conducted by a three-electrode system. The conductivity of TTF-COP (2.5×10^{-6} S/cm) exhibits about 200 times higher than that of PVDF (1.3×10^{-8} S/cm), supporting the superior role of TTF unit in enhancing the battery performance (Fig. S25 in Supporting information) [17,62].

Subsequently, TTF-COP based electrode was prepared by one-pot fabrication of cathode *via in-situ* polymerization of TTF-COP monomers to combine S and CNT (details see Supporting information). Thermogravimetric analysis determines the S content in the electrode is approximately 49 wt% (Fig. S26 in Supporting information). The electrochemical performance of cathodes based on TTF-COP, TPA-COP and PVDF were compared through control experiments. For TTF-COP based cathode, CV curves display two typical reduction peaks at 2.31 and 1.97 V with a scan rate of 0.1 mV/s, representing the transitions from solid-state S_8 to soluble LiPSs and from LiPSs to insoluble Li_2S_2/Li_2S, respectively. Besides, two oxidizing peaks at 2.41 V and 2.48 V, corresponding to the reverse process of LiPSs back to S are observed (Fig. 4a). The oxidation peak at 2.41 V corresponds to the transformation of Li_2S into Li_2S_n ($n = 2–8$) and the oxidation peak at 2.48 V is ascribed to the transformation of Li_2S_n ($n = 2–8$) into S_8 [3,63–65]. The higher intensity of TTF-COP/CNT/S in CV curves manifests more favorable reaction kinetics than TPA-COP and PVDF (Figs. S27-S29 in Supporting information). Corresponding to the CV results, the constant current charge-discharge curves of the cells based on these binders consist of two clear discharging platforms and one charging platform (Figs. S30-S32 in Supporting information). In addition, TTF-COP/CNT/S has a small overpotential for the conversion from long chain LiPSs to insoluble Li_2S_2/Li_2S (Fig. 4b).

Besides, The rate capabilities of LSBs are investigated at various rates ranging from 0.1 C to 2 C, and back to 0.2 C (Fig. 4c). TTF-COP/CNT/S presents stable rate capability of 1173.7, 857.0, 775.7, 720.1, 649.8, 600.0, 558.2 mAh/g at 0.1, 0.2, 0.3, 0.5, 1, 1.5 and 2 C, respectively, which is better than PVDF/CNT/S (1049.7, 588.2, 497.7, 446.3, 388.5, 341.9 and 308.8 mAh/g, respectively). In addition, when the current density of TTF-COP/CNT/S is directly decreased back to 0.2 C, its capacity retains at 727.2 mAh/g, indicating its superior high-rate performance. As comparison, TPA-COP/CNT/S and PVDF/CNT/S shows lower capacity than that of TTF-COP/CNT/S under different current densities. As presented in Fig. 4d, good cycling stability can be achieved by TTF-COP/CNT/S with initial discharge specific capacity of 1125.7 mAh/g at 0.5 C.

In contrast, TPA-COP/CNT/S and PVDF/CNT/S exhibit lower initial discharge specific capacity of 920.2 and 728 mAh/g, respectively. The introduction of TTF unit increases the initial discharge capacity of TTF-COP/CNT/S from 920.2 mAh/g to 1125.7 mAh/g when compared to TPA unit. Notably, the TTF-COP/CNT/S can light up an LED panel (Fig. 4e). TTF-COP/CNT/S exhibits excellent initial discharge capacities of 927.6 and 717.4 mAh/g at 1 and 2 C with the capacity decay of 0.126% and 0.076% per cycle after 200 cycles, respectively (Figs. S33 and S34 in Supporting information). It is worth mentioning that TTF-COP/CNT/S can deliver a discharge capacity of 572.1 mAh/g at 5 C and the Coulombic efficiency is nearly 100% (Fig. 4e). At 6 C, TTF-COP/CNT/S can still exhibit moderate discharge performance with a 52.6% capacity retention after 100 cycles (Fig. S35 in Supporting information). We have further performed the galvanostatic intermittent titration technique (GITT) discharge process tests, and the results show that the sulfur utilization of the TTF-COP/CNT/S (71.2%) is higher than that of PVDF/CNT/S (55.6%) (Fig. S36 in Supporting information). High sulfur loading and E/S ratio have become critical indicators for evaluating the practical application of LSBs. Based on this, TTF-COP/CNT/S with a comparatively high sulfur loading of 4.2 mg/cm^2 and a low E/S ratio (12.1 μL/mg) exhibits a high specific capacity of 3.7 mAh/cm^2, which could further be stabilized at 2.1 mAh/cm^2 after 150 cycles (Fig. S37 in Supporting information). When the sulfur loading is 5.9 mg/cm^2, and the E/S ratio is as low as 8.6 μL/mg, it can still deliver an outstanding capacity of 3.9 mAh/cm^2 and can be kept at 2.7 mAh/cm^2 after 40 cycles (Fig. S38 in Supporting information). Furthermore, even when the sulfur loading is as high as 7.1 mg/cm^2, it still demonstrates an excellent capacity of 5.1 mAh/cm^2 and can be maintained at 3.9 mAh/cm^2 after 25 cycles (Fig. S39 in Supporting information). Notably, the TTF-COP/CNT/S exhibits excellent performance to the most of reported binders used as LSBs (Tables S2 and S3 in Supporting information).

In addition, different contents (5–20 wt%) of binders have also been studied to explore the optimal specific gravity of 10 wt% binder in the cathode (Figs. S40 and S41 in Supporting information). The batteries using these conventional polymer binders (such as sodium alginate and sodium carboxymethylcellulose) exhibit significant capacity decay after 200 cycles at 0.5 C, further demonstrating the advantage of TTF-COP in stabilizing electrochemical performance (Fig. S42 in Supporting information). Additionally, SEM images reveal that the surfaces of cycled TPA-COP/CNT/S and PVDF/CNT/S become rough with apparent cracks. Notably, the surface of TTF-COP/CNT/S remains uniform and smooth, which indicates that the high mechanical strength of TTF-COP significantly contributes to the stability of electrode (Figs. S43 and S44 in Supporting information). Furthermore, the SEM cross-section images confirm that TTF-COP/CNT/S buffers volume changes of the sulfur active material during the cycling process, compared with PVDF/CNT/S (Figs. S45 and S46 in Supporting information). In short, the TTF-COP as a multifunctional binder, not only maintains excellent cycling stability due to enhanced mechanical strength but also achieves the adsorption and conversion of LiPSs by redox-active center of TTF.

In summary, we have designed a kind of redox and conductive binder (TTF-COP) by *in-situ* polymerization of redox/conductive tetrathiafulvalene unit and adhesive thiourea unit. TTF-COP can achieve one-pot cathode fabrication and simultaneously provide strong interactions with cathodic materials, showing significantly enhanced mechanical strength of the electrode, accelerating capture/conversion of LiPSs, about 10^4 times higher viscosity (at shear rates of 0.1–1 s^{-1}), and about 200 times enhanced electrical conductivity than that of PVDF. The battery based on TTF-COP/CNT/S delivers initial specific capacities of 1126, 928, 611 mAh/g at 0.5, 1 and 5 C, respectively, and excellent cycling stability with over 800 cycles at 5 C (0.089% decay per cycle and the Coulombic efficiency is nearly 100%). Moreover, the cell shows an excellent specific capacity of 5.1 mAh/cm^2 under a high sulfur loading of 7.1 mg/cm^2 and low E/S ratio of 10.7 μL/mg. Besides, theoretical calculation reveals the vital roles of tetrathiafulvalene and thiourea units in enhancing the battery-performance. The research might provide a new reference for the development of powerful binders for portable electronic devices.

CRediT authorship contribution statement

Taoping Huang: Writing – review & editing, Writing – original draft, Investigation, Conceptualization. **Xiaoman Yao:** Writing – original draft, Investigation. **Xuanxu Chen:** Investigation. **Minqiao Liang:** Software. **Mingjin Shi:** Resources. **Yiwen Yang:** Investigation. **Fei Yu:** Software, Methodology. **Fengxue Duan:** Writing – original draft, Project administration, Conceptualization. **Yifa Chen:** Writing – review & editing, Supervision, Project administration, Funding acquisition, Conceptualization. **Ya-Qian Lan:** Funding acquisition.

Declaration of competing interest

The authors declare that they have no known competing financial interests or personal relationships that could have appeared to influence the work reported in this paper.

Acknowledgments

This work was financially supported by the National Key R&D Program of China (No. 2023YFA1507204). National Natural Science Foundation of China (Nos. 22475074, 22171139, 22225109). Guangdong Provincial Key Laboratory of Carbon Dioxide Resource Utilization (No. 2024B1212010011). Major Research Plan of the National Natural Science Foundation of China (No. 92461310). Natural Science Foundation of Guangdong Province (No. 2023B1515020076). The Double Thousand Talents Plan of Jiangxi Province (No. jxsq2023102003).

Supplementary materials

Supplementary material associated with this article can be found, in the online version, at doi:10.1016/j.cclet.2025.111414.

References

[1] P.G. Bruce, S.A. Freunberger, L.J. Hardwick, J.M. Tarascon, Nat. Mater. 11 (2012) 19–29.
[2] A. Manthiram, Y. Fu, S.H. Chung, C. Zu, Y.S. Su, Chem. Rev. 114 (2014) 11751–11787.
[3] L. Zhang, T. Qian, X. Zhu, et al., Chem. Soc. Rev. 48 (2019) 5432–5453.
[4] Z.W. Seh, Y. Sun, Q. Zhang, Y. Cui, Chem. Soc. Rev. 45 (2016) 5605–5634.
[5] S. Zhou, J. Shi, S. Liu, et al., Nature 621 (2023) 75–81.
[6] G. Zhou, H. Chen, Y. Cui, Nat. Energy 7 (2022) 312–319.
[7] C.L. Song, Z.H. Li, L.Y. Ma, et al., ACS Nano 15 (2021) 13436–13443.
[8] L. Su, N. Yao, Z. Li, et al., Angew. Chem. Int. Ed. 63 (2024) e202318785.
[9] W. Yao, J. Xu, L. Ma, et al., Adv. Mater. 35 (2023) 2212116.
[10] Y. Kong, X. Qiu, Y. Xue, et al., J. Am. Chem. Soc. 146 (2024) 23764–23774.
[11] X. Yao, C. Guo, C. Song, et al., Adv. Mater. 35 (2023) 2208846.
[12] W. Wang, L. Hua, Y. Zhang, G. Wang, C. Li, Angew. Chem. Int. Ed. 63 (2024) e202405920.
[13] R. Sun, J. Hu, X. Shi, et al., Adv. Funct. Mater. 31 (2021) 2104858.
[14] F. Zou, A. Manthiram, Adv. Energy Mater. 10 (2020) 2002508.
[15] K. Yang, L. Yang, Z. Wang, et al., Adv. Energy Mater. 11 (2021) 2100601.
[16] C. Guo, M. Liu, G. Gao, et al., Angew. Chem. Int. Ed. 61 (2022) e202113315.
[17] J. Chen, X. Geng, C. Wang, et al., J. Mater. Chem. A 12 (2024) 11038–11048.
[18] N. Lingappan, L. Kong, M. Pecht, Renew. Sustain. Energy Rev. 147 (2021) 111227.
[19] C. Senthil, S.S. Kim, H.Y. Jung, Nat. Commun. 13 (2022) 145.
[20] R. Guo, S. Zhang, H. Ying, et al., ACS Appl. Mater. Interfaces 11 (2019) 14051–14058.
[21] C. Li, Q. Sun, Q. Zhang, et al., Chem. Eng. J. 455 (2023) 140706.
[22] Y. Li, J. Chen, P. Cai, Z. Wen, J. Mater. Chem. A 6 (2018) 4948–4954.
[23] R. Guo, S. Zhang, J. Wang, H. Ying, W. Han, ChemSusChem 13 (2020) 819–826.

[24] C. Wang, P. Chen, Y. Wang, et al., Adv. Funct. Mater. 32 (2022) 2204451.
[25] M. Li, H. Chen, C. Guo, et al., Adv. Energy Mater. 13 (2023) 2300646.
[26] J. Su, S. Yuan, H.Y. Wang, et al., Nat. Commun. 8 (2017) 2008.
[27] Y. Shiina, Y. Kage, K. Furukawa, et al., Angew. Chem. Int. Ed. 59 (2020) 22721–22730.
[28] Q. Li, J.N. Chang, Z. Wang, et al., J. Am. Chem. Soc. 145 (2023) 23167–23175.
[29] T. Yan, Y.Y. Li, J. Su, H.Y. Wang, J.L. Zuo, Chem. Eur. J. 27 (2021) 11050–11055.
[30] S.W. Ke, Y. Wang, J. Su, et al., J. Am. Chem. Soc. 144 (2022) 8267–8277.
[31] X. Zhou, C. Liu, J. Su, et al., Angew. Chem. Int. Ed. 62 (2023) e202211850.
[32] S. Lv, X. Ma, S. Ke, et al., J. Am. Chem. Soc. 146 (2024) 9385–9394.
[33] J. Zhang, B. Sun, Y. Zhao, K. Kretschmer, G. Wang, Angew. Chem. Int. Ed. 56 (2017) 8505–8509.
[34] K. Kikkawa, Y. Sumiya, K. Okazawa, et al., J. Am. Chem. Soc. 146 (2024) 21168–21175.
[35] Z. Zhang, H. Peng, M. Zhao, J. Huang, Adv. Funct. Mater. 28 (2018) 1707536.
[36] G. Li, X. Wang, M.H. Seo, et al., Nat. Commun. 9 (2018) 705.
[37] H. Yuan, J. Huang, H. Peng, et al., Adv. Energy Mater. 8 (2018) 1802107.
[38] T. Zhang, B. Li, Z. Song, et al., Energy Environ. Mater. 7 (2024) e12572.
[39] Y.L. Yang, Y.R. Wang, G.K. Gao, et al., Chin. Chem. Lett. 33 (2022) 1439–1444.
[40] M. Lu, J. Liu, Q. Li, et al., Angew. Chem. Int. Ed. 58 (2019) 12392–12397.
[41] J. Chang, Q. Li, J. Shi, et al., Angew. Chem., Int. Ed. 62 (2023) e202218868.
[42] R.X. Yang, Y.R. Wang, G.K. Gao, et al., Small Struct. 2 (2021) 2100012.
[43] D. Chen, M. Song, M. Zhu, et al., ACS Appl. Energy Mater. 5 (2022) 5287–5295.
[44] Y. Zuo, R. Liu, X. Zhang, et al., Chem. Commun. 55 (2019) 13924–13927.
[45] R.Y. Wang, H. Kang, M.J. Park, ACS Appl. Energy Mater. 4 (2021) 2696–2706.
[46] A. Kawase, S. Yamazaki, Y. Kamishima, R. Tatara, S. Komaba, ACS Appl. Energy Mater. 7 (2024) 2057–2068.
[47] R. Guo, J. Wang, S. Zhang, W.Q. Han, Chem. Eng. J. 388 (2020) 124316.
[48] M. Zheng, X. Cai, Y. Tan, et al., Chem. Eng. J. 389 (2020) 124404.
[49] M. Zhang, S. Geng, G. Yan, et al., J. Colloid Interface Sci. 633 (2023) 1–10.
[50] J. Qiu, S. Wu, Y. Yang, et al., ACS Appl. Mater. Interfaces 13 (2021) 55092–55101.
[51] Y.P. Chuang, J.L. Hong, ACS Appl. Energy Mater. 4 (2021) 10213–10221.
[52] Y. Feng, H. Liu, F. Zhao, et al., Chem. Eng. J. 409 (2021) 128177.
[53] S. Chen, Z. Song, Y. Ji, et al., Small Methods 5 (2021) 2100839.
[54] Y. Wen, X. Lin, X. Sun, et al., J. Colloid Interface Sci. 660 (2024) 647–656.
[55] Y. Jia, W. Gong, X. Fan, et al., Chem. Eng. J. 444 (2022) 136546.
[56] J. Wang, X. Chen, Z. Wang, et al., Chem. Eng. J. 465 (2023) 142657.
[57] B. Li, T. Zhang, Z. Song, et al., Adv. Funct. Mater. 33 (2023) 2306990.
[58] M. Si, X. Jian, Y. Xie, et al., Adv. Energy Mater. 14 (2024) 2303991.
[59] Z. Chen, T. Chen, J. Wang, et al., Adv. Energy Mater. 14 (2024) 2401568.
[60] Y. Jiang, S. Liu, X. Gao, G. Li, Adv. Funct. Mater. 33 (2023) 2304965.
[61] Q. Gong, L. Hou, T. Li, Y. Jiao, P. Wu, ACS Nano 16 (2022) 8449–8460.
[62] B. Jin, L. Yang, J. Zhang, et al., Adv. Energy Mater. 9 (2019) 1902938.
[63] C. Ma, Y. Zhang, Y. Feng, et al., Adv. Mater. 33 (2021) 2100171.
[64] J. Lei, X.X. Fan, T. Liu, et al., Nat. Commun. 13 (2022) 202.
[65] D. Wang, Y. Jia, Q. Jin, et al., Adv. Sci. 12 (2025) 2412038.